



Synthesis, characterization and activity of photocatalytic sol–gel TiO₂ powders and electrodes

Javier Marugán^{a,b,*}, Paul Christensen^b, Terry Egerton^b, Herry Purnama^b

^a Department of Chemical and Environmental Technology, ESCET, Universidad Rey Juan Carlos, C/Tulipán s/n, 28933 Móstoles, Madrid, Spain

^b School of Chemical Engineering and Advanced Materials, Newcastle University, Bedson Building, Newcastle Upon Tyne, NE1 7RU, UK

ARTICLE INFO

Article history:

Received 1 December 2008

Received in revised form 9 February 2009

Accepted 13 February 2009

Available online 21 February 2009

Keywords:

Sol–gel

Titania

Iron doping

Electrodes

Photocatalysis

Photoelectrocatalysis

Reactive Orange 16

ABSTRACT

The efficiency of photoelectrocatalytic processes is strongly influenced by the electrode type and synthesis procedure. This work reports the sol–gel synthesis and characterization of TiO₂ and Fe-doped TiO₂ powders and electrodes as a function of pH and preparation temperatures and the correlation of their photoelectrochemical properties with their activity for azo dye decolourisation. pH is shown to be the variable that most influences the formation of the TiO₂ crystalline phases, the photocurrents of the electrodes, and consequently their photocatalytic activity.

Electrodes synthesized at low pH and heated at temperatures below ~600 °C show a significant increase in the photocurrent recorded in the presence of methanol. This is attributed to suppression of the charge recombination rather than to a conventional current-doubling mechanism. The photocatalytic activities of the electrodes show a good correlation with the photocurrent measured in the presence of methanol. The mechanistic implications of this correlation are discussed.

Iron doping reduces the activity of the sol–gel electrodes for dye decolourisation. This contrasts with previous results for bacteria disinfection, which is believed to proceed by a hydroxyl radical mechanism. Consequently, it may be that the behaviour of iron as recombination centres or as trapping sites that improve the separation charges may depend on whether the photoelectrocatalytic reaction proceeds by a hydroxyl radical mechanism, as was shown for deactivation of *Escherichia coli* or by direct hole-transfer, as is suggested by the parallels between dye decolouration and the electrode response to methanol that are reported in this paper.

© 2009 Elsevier B.V. All rights reserved.

1. Introduction

The heterogeneous photocatalytic oxidation of many chemical pollutants has been reported, and the fundamentals of this semiconductor-mediated photochemical-degradation of contaminants have been extensively reviewed in recent decades [1–8]. TiO₂ slurries have been shown to be highly active for water detoxification and allow simple dosing and reactor operation. However, the commercial application of photocatalytic water treatment has been hindered both by difficulties of post-reaction catalyst recovery [9] and by low quantum efficiencies [10], which means that large reactors are required for small capacity plants. Both problems may be addressed by immobilization of TiO₂ on a conducting support and application of a potential bias, leading to the so-called photoelectrocatalytic process [11,12].

The application of a small positive potential to a semiconductor increases the potential gradient within the depletion layer formed

near to the TiO₂/solution interface. UV radiation excites electrons to the semiconductor conduction band where they are attracted by the positive potential of the back of the anode and conducted by the external circuit to the cathode where reduction reactions can occur. Simultaneously, the positive holes in the valence band migrate to the TiO₂/solution interface where they can oxidize organics. Thus, the applied potential improves charge separation and reduces unproductive recombination processes. Several research groups have reported the photoelectrocatalytic degradation of different organic pollutants [13–20] and also the disinfection of bacteria suspensions [21,22].

The efficiency of photoelectrocatalytic processes is highly dependent on the electrode type and synthesis procedure [21–24]. A common preparation of TiO₂ electrodes is to coat conducting materials with titania sol–gel suspensions, and this procedure provides fine control of the physicochemical properties, and hence of the photocatalytic activity, of the TiO₂ crystalline phase [25]. Three critical variables in sol–gel coating preparations are (i) the temperature of the heat treatment used to crystallize the titania [21]; (ii) the presence of metal ion dopants on the semiconductor network [22]; and (iii) the pH of the synthesis and coating suspensions [26].

* Corresponding author. Tel.: +34 91 664 7466; fax: +34 91 488 7068.

E-mail address: javier.marugan@urjc.es (J. Marugán).

This study correlates the photocatalytic and photoelectrocatalytic activity with the physicochemical and electrochemical properties of sol–gel TiO₂-coated titanium electrodes synthesized using two different pH routes, different heat-treatment temperatures and variations in iron doping. Iron was selected as it has been reported to increase the TiO₂ photoreactivity for both oxidation and reduction reactions [27] and for photoelectrocatalytic disinfection [22]. The study has followed successive steps of powder preparation, followed by small test-electrodes preparation and finally large mesh electrode fabrication.

2. Experimental

2.1. Synthesis of the powder catalysts and electrodes

Titanium dioxide sols were prepared following a procedure based on that of O'Regan et al. [28]. 50 mL of titanium tetrakisopropoxide (TTIP) (97%, Aldrich) was mixed with 8 mL of 2-propanol (ACS Reagent, Riedel-de Haën) and added dropwise to 300 mL of deionized water (18.2 MΩ cm) under vigorous stirring to form a white precipitate. Iron-doped TiO₂ suspensions were prepared by dissolving iron(III) acetylacetonate (99.9%, Aldrich) in the initial 2-propanol solution. At that point, the pH of the acid suspensions was adjusted by slowly adding 2.12 mL of nitric acid 70% prior to refluxing for 8 h at 80 °C. This peptization process yielded a stable TiO₂ colloidal suspension.

The derived powders were separated by increasing the pH of the colloidal suspensions to 6.5 with sodium hydroxide prior to vacuum-filtering the suspension through a 2.7 μm paper filter (Whatman Grade 542). The filter cake was resuspended in deionized water three times, to remove the ions from the solution, until the filtrate conductivity fell below 200 μS cm⁻¹, and finally was rinsed twice with 2-propanol to minimize particle agglomeration. Removal of ions from the powders was confirmed by measurement of the sodium content of the materials by inductively coupled plasma atomic emission spectroscopy (ICP-AES) in a Varian Vista AX instrument. The solids were dried at room temperature and then calcined at the desired temperature.

To prepare the electrodes, the viscosity of the colloidal suspension was first increased by concentration to ca. 150 g L⁻¹ titania, using a vacuum rotary evaporator. Small thin-film electrodes were fabricated by dropping suspension onto 1 cm × 1 cm titanium plates (99.6%, Goodfellow) which were spun at 2800 rpm prior to calcination for 10 min at the desired temperature. The dropping, spinning and heating sequence were repeated five times. Large electrodes were fabricated by dipping a cylindrical titanium mesh (Expamet, 42% open area, 1.5 mm × 1 mm diamond-shaped holes) into the concentrated titania suspension, followed by draining, spinning horizontally at

2800 rpm, and calcining. This sequence was also repeated five times.

2.2. Characterization techniques

X-ray diffraction (XRD) patterns of both the powder materials and the small plate electrodes were collected in the range 10° < 2θ < 90° in a Philips X'Pert diffractometer using nickel filtered monochromatic Cu Kα radiation. The average size of TiO₂ crystallites was estimated from the broadening of the main X-ray diffraction signals (anatase 1 0 1 at 2θ ~ 25.3° and rutile 1 1 0 at 2θ ~ 27.4°) using Scherrer's equation.

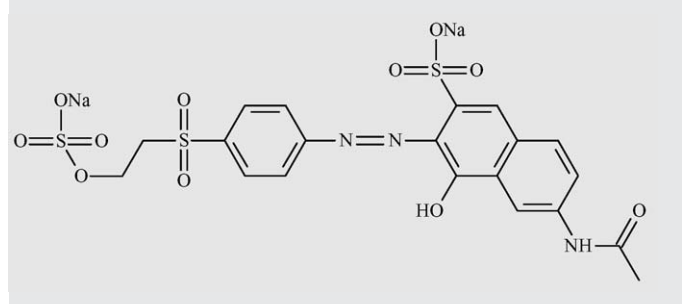
The BET specific surface areas of the samples were calculated from the nitrogen adsorption–desorption isotherms at 77 K obtained in a Micromeritics Tristar 3000 equipment. Thermal analysis of the precursor sols were carried out in a Setaram Setsys 18A TG-DTA instrument using air as carrier gas and a heating ramp of 5 °C min⁻¹.

The incorporation of iron into the powder Fe/TiO₂ materials was determined by inductively coupled plasma atomic emission spectroscopy (ICP-AES) in a Varian Vista AX instrument. The catalysts were dissolved by attack with hydrofluoric acid and rinsed to a 50 mL volume with deionized water. The iron concentration in the solution was quantified through its emission lines at 238.204 and 259.940 nm after calibration with certified standards. The iron-doped samples are yellowish-brown which indicates a shift of the absorption edge to the visible, which is characteristic of iron doping. Possible enhancements of 'visible photocatalysis' associated with this effect have not been addressed in order to focus on the comparison of UV photocatalysis by doped and undoped samples.

The morphology of the TiO₂ films on the coated electrodes was investigated by scanning electron microscopy (SEM) on a JEOL JSM5300LV. By working at an acceleration voltage of 25 kV under environmental conditions, the use of a conductive coating on the sample was avoided.

Electrochemical characterization was carried out on the small plate electrodes by cyclic voltammetry, with a sweep rate of 100 mV s⁻¹, using an Eco-Chemie μAutolab Type II potentiostat. Potentials were quoted with respect to an Ag/AgCl reference electrode and a nickel gauze (99%, Goodfellow) of 10 cm in diameter was employed as counter electrode. As electrolyte, a 0.1 M solution of Na₂SO₄ (99%, Riedel-de Haën) was used. Methanol was obtained from Riedel-de Haën (99.8%). The electrochemical cell consists of a jacketed cylindrical vessel made of Pyrex glass. Illumination was performed by two 36 W actinic UV lamps (Philips CLEO Compact) located above, whereas cooling water was circulated through the jacket to prevent overheating and maintain a constant temperature [12]. Differences between

Table 1
Structure of Reactive Orange 16 (RO16), wavelength of the absorption maximum and experimental extinction coefficient at this wavelength determined by calibration.

Structure	λ _{max} (nm)	ε (mol ⁻¹ dm ³ cm ⁻¹)
	493	23,450

the responses of the electrodes in dark and illuminated conditions were used to estimate the UV-induced photocurrent as function of the applied potential.

2.3. Photoreactions procedure

Decolourisation of the azo-dye Reactive Orange 16 (RO16) (Table 1) was used as a model reaction to evaluate the photocatalysts. The 0.05 mM dye solutions were prepared using deionized water; the photoelectrocatalytic experiments were conducted in 0.1 M Na_2SO_4 solutions. The solution obtained after dissolving the dye was used without further pH adjustment.

The suspension of catalyst in the dye solution was contained within the annulus between the two concentric Pyrex tubes and was illuminated by two 8 W UV lamps (Sylvania Black Light 350 F8W/T5/BL350) located in the axial well. The suspension was sparged by oxygen via a sintered frit at the bottom of the reactor. For photocatalytic experiments, the TiO_2 was suspended in the dye solution; for photoelectrocatalytic studies a two mesh-electrode cassette was placed within the annular volume with the TiO_2 electrode closer to the lamps. More details about the reactor can be found elsewhere [21].

The initial 0.05 mM dye solutions were equilibrated in the dark for 30 min in contact with the TiO_2 and oxygen bubbles prior to the start of the reaction. After switching on the lamps, the evolution of the reaction was followed by colorimetric measurements using a Shimadzu UV/Vis spectrophotometer (see Table 1 for calibration results).

3. Results and discussion

3.1. Powder photocatalysts

The increased sharpness of the powder diffractograms (Fig. 1) of pure titania powder photocatalysts synthesized in acidic media demonstrate that after calcination at 500 °C the TiO_2 exists as small crystallites of anatase which grow substantially and partially transform to rutile, as evidenced by the growth of the rutile maximum at $2\theta \sim 27.4^\circ$, after calcination at 600 °C. The extent of rutilisation is higher for longer heat treatments.

A similar study was carried out for titania materials doped with 0.1 at.% and 0.5 at.% iron (Fig. 2). Only anatase and rutile crystalline

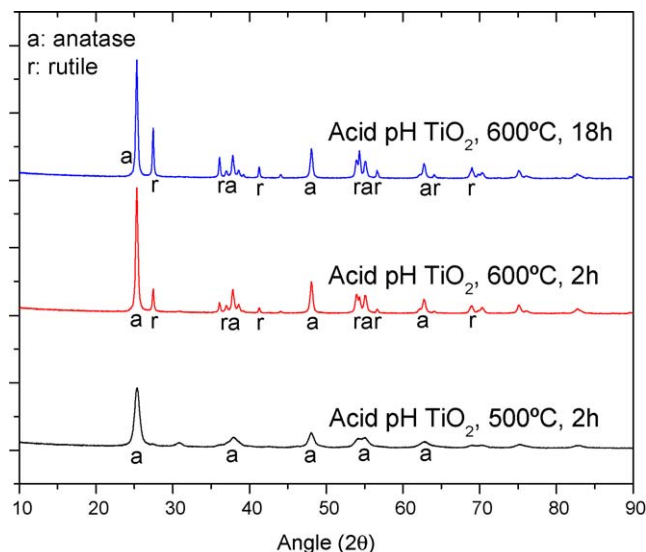


Fig. 1. X-ray diffraction pattern of pure titania powder photocatalysts prepared under acidic conditions.

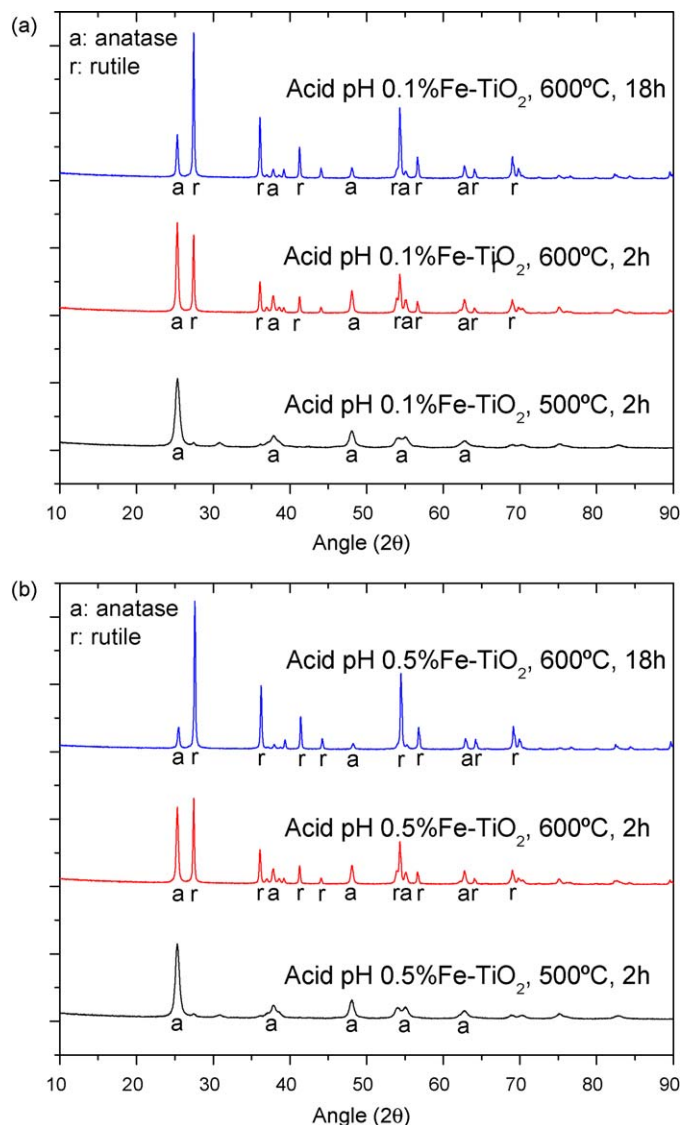


Fig. 2. X-ray diffraction pattern of iron doped titania powder photocatalysts, prepared under acidic conditions.

phases were detected, suggesting the incorporation of the doping ions into the titania crystal structure. However, the iron content is very low and consequently the formation of iron-containing crystalline phases could be not detectable. Again, the material calcined at 500 °C consists exclusively of anatase, whereas a significant transformation to rutile – much more than for pure titania and greater for the higher iron level – was observed after heat treatments at higher temperatures and for longer durations. The mass percentage of anatase has been calculated from the intensity ratio of the diffraction-maxima of anatase (101 ; $2\theta \sim 25.3^\circ$) and rutile (110 ; $2\theta \sim 27.4^\circ$) using the relationship $\text{anatase (wt.\%)} = 0.884A_{\text{anatase}} / (0.884A_{\text{anatase}} + A_{\text{rutile}})$ [29]. Table 2 summarizes the results of the crystalline analyses and of the average crystallite sizes estimated from line broadening [25].

Table 2 also summarizes the XRD characterization and the photocatalytic activity for samples prepared, using nitric acid, at pH 1.5 and also for those prepared in neutral aqueous media. (As a shorthand pH 6.5 will be referred to in the remaining text as 'neutral' to differentiate it from the acid pH 1.5.) Synthesis at neutral pH leads to anatase, exclusively [26] as implied by reports that low pH favours rutile formation [30] and to a smaller average crystal size. For both sets of samples the average crystallite size of

Table 2

Synthesis conditions, crystallinity and photocatalytic activity in terms of the first order kinetic constant for RO16 decolourisation of powder photocatalysts prepared at pH 1.5 and, in brackets, pH 6.5.

Sample code	% Fe	Temperature (°C)	XRD data		k_{RO} (h ⁻¹) ^{a,b}
			Anatase (%)	D_{anat} (nm)	
P-TiO ₂ -1 (-4)	0	500/2 h	100 (100)	14 (12)	0.22 (0.38)
P-TiO ₂ -2 (-5)	0	600/2 h	89 (100)	42 (24)	0.32 (1.09)
P-TiO ₂ -3 (-6)	0	600/18 h	76 (100)	50 (26)	0.32 (0.60)
P-FeTiO ₂ -1 (-7)	0.1	500/2 h	98 (100)	17 (21)	0.10 (0.17)
P-FeTiO ₂ -2 (-8)	0.1	600/2 h	60 (100)	49 (25)	0.16 (0.22)
P-FeTiO ₂ -3	0.1	600/18 h	25	65	0.08
P-FeTiO ₂ -4 (-9)	0.5	500/2 h	98 (100)	18 (24)	0.09 (0.07)
P-FeTiO ₂ -5 (-10)	0.5	600/2 h	54 (100)	48 (29)	0.10 (0.04)
P-FeTiO ₂ -6	0.5	600/18 h	13	69	–

^a All the reactions were carried out with a catalyst concentration of 0.5 g L⁻¹.

^b The values of k_{RO} obtained with suspensions of commercial TiO₂ samples Degussa P25 and Millenium PC500 under the same experimental conditions are 2.82 and 0.18 h⁻¹, respectively.

anatase increased significantly with calcination temperature and with iron content, from 14 nm for pure titania prepared at pH 1.5 and calcined at 500 °C to 69 nm for 0.5% Fe doped titania calcined at 600 °C for 18 h. A plot of anatase crystallite size as a function of % anatase – see Fig. 3 – is consistent with the widely accepted mechanism that anatase transforms to rutile when the higher surface energy no longer compensates for its higher free energy of formation [31] and demonstrates why the smaller crystals, formed at neutral pH, are 100% anatase even after calcination at 600 °C. These results imply that the role of iron is primarily to promote crystal growth rather than acting as a specific rutilising agent.

ICP-AES analysis confirmed that the incorporation of iron with respect to the nominal content is almost total (>97%) for both pH values of synthesis. However, that not means that iron is homogeneously distributed on the titania particles. The reason is that the hydrolysis of iron and titanium precursors can take place at different rates, usually leading to lower iron content on the external surface of titania, as confirmed by the XPS analysis reported by Navío et al. [32].

Thermal analysis of the precursor sols of the materials by TG-DTA (not shown) does not evidence significant differences depending on the pH or the presence of iron. All the curves exhibit an important weight loss through a endothermic process corresponding to the solvent removal below 250 °C, followed by a exothermic signal derived of the combustion of the organic residuals and a less intense exothermic signal corresponding to the

crystallization of anatase that finish around 460 °C. Above 460 °C no significant weight losses or thermal processes are observed suggesting that no important differences should be expected between materials calcined at 500 and 600 °C apart from the crystalline transition from anatase to rutile.

As examples of the photocatalytic activity, the decrease in dye concentration with increasing radiation time is shown for four representative materials in Fig. 4. For all catalysts, the results were

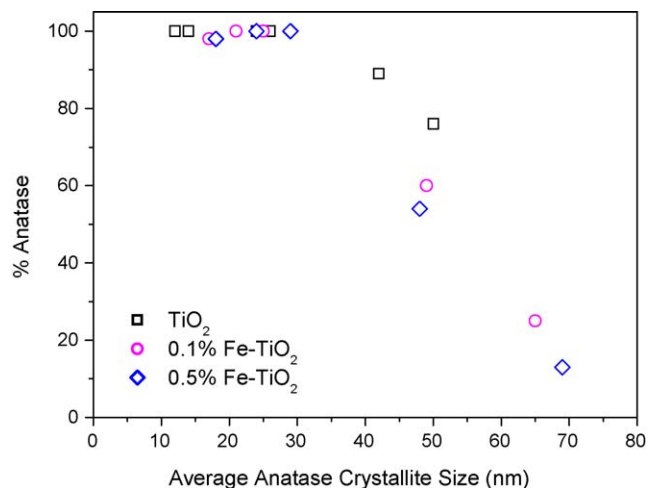


Fig. 3. Experimental relation between the percentage of anatase and the average crystallite size for pure and iron-doped titania powders.

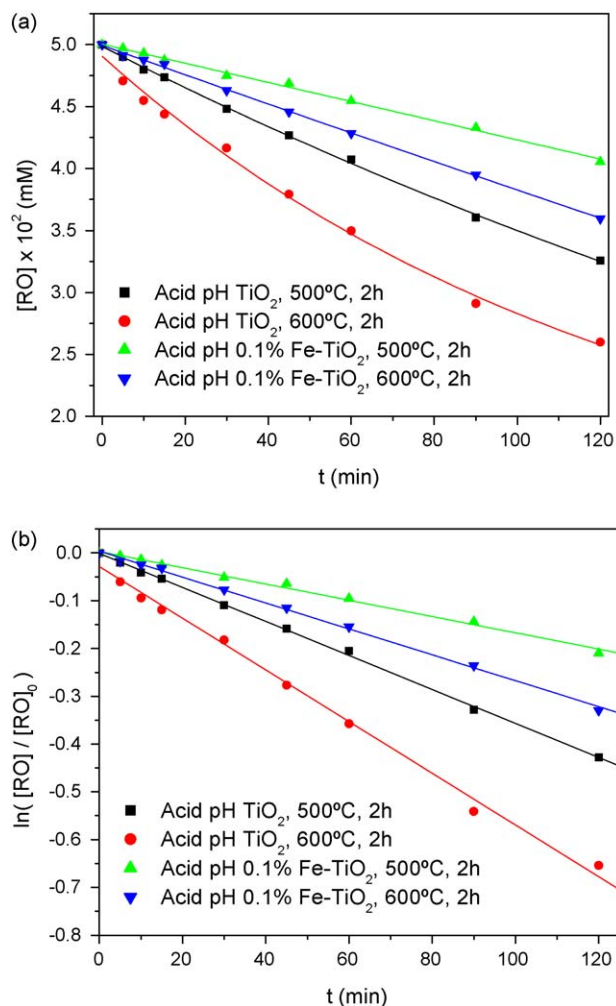


Fig. 4. Decolouration and derived first order kinetics fit of the RO16 photocatalytic decolourisation with powder photocatalysts.

satisfactorily represented by pseudo-first order kinetics and the derived rate constants are listed in Table 2. It can be noticed that the activity of all the samples is lower than that achieved by suspensions of Degussa P25, but is comparable to the activity of Millenium PC500 suspensions.

The exclusively anatase catalysts prepared by the sol–gel route at pH 6.5 are considered first. (The results are shown in brackets in Table 2.) The photoactivity for dye decolouration of these powders was generally higher than that of otherwise equivalent powders prepared at pH 1.5. Considering that the BET surface area of both types of powders are quite similar (in the range of 15–21 m² g^{−1} depending on the calcination temperature), this may be partially attributed to the smaller crystallite size of anatase and to the consequent absence of rutile. Doping with 0.1 and 0.5% iron reduced the apparent rate constant for dye degradation. This implies that the increased charge-carrier recombination associated with iron recombination centres in the bulk of the crystal is more important than charge separation by e.g. electron trapping at Fe³⁺ centres in the catalyst surface. (In earlier studies recombination became dominant in the range 0.1–0.5 at.%. [22]). In addition, for the undoped and the 0.1% Fe doped neutral powders, an increase in the calcination temperature from 500 to 600 °C increased the activity even though the sharper XRD diffraction lines imply the expected increase in crystallite size at the higher temperature. Crystal growth would lower the catalyst area and hence decrease dye degradation (which

is generally considered to involve reaction of an adsorbed dye molecule). However, sharpening of the diffraction patterns of samples heated at higher temperatures can be due not only to crystal growth, but also to improved crystallinity [25]. It is suggested that this improved crystallinity, decreases the number of intrinsic recombination centres and therefore increases photocatalytic activity. For the highly doped, 0.5% Fe, crystals activity decreases with increasing calcinations – presumably because the extrinsic recombination centres associated with iron reduce the relative benefits of a decreased number of intrinsic recombination defects associated with improved crystallinity and therefore the effect of decreasing surface area dominates.

Although the photoactivity of samples prepared at pH 1.5 was generally lower than that of neutral powders, iron doping again significantly reduced photoactivity. Thus in both sets of samples the dominant role of the iron has been to introduce recombination centres rather than to improve charge separation. This conclusion is in agreement with those reported by several research groups [33–35] although other authors have reported the opposite behaviour, with optimal doping levels varying widely from 0.05 at.% [36] to 0.5 at.% [27] and 0.7 at.% [37]. It is probable that changes in the relative importance of bulk and surface recombination, caused not only by surface area differences but also by changes in the degree of crystallinity, contribute to the extreme sensitivity of iron doping to the synthesis conditions.

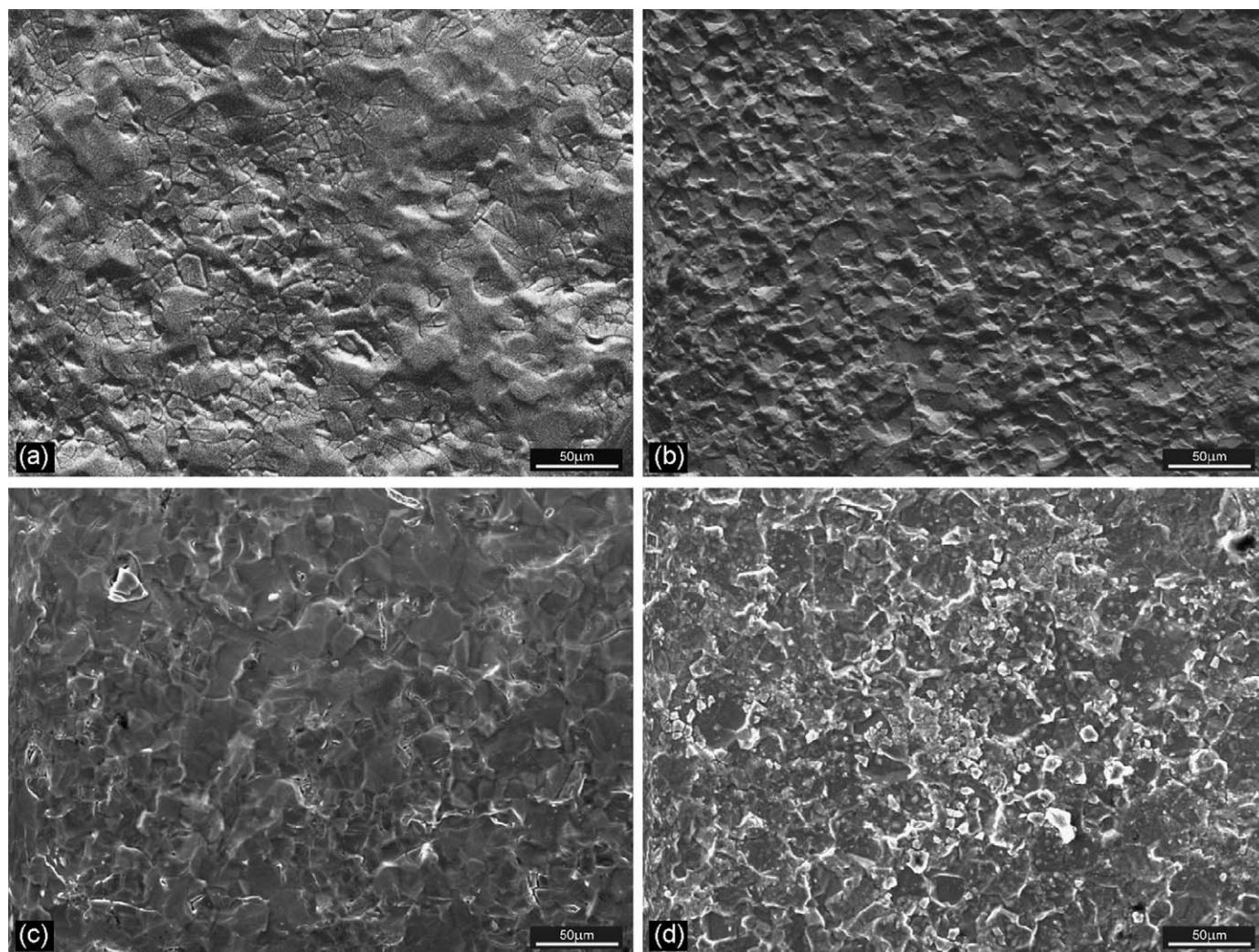


Fig. 5. SEM micrographs spectra of TiO₂ electrodes: (a) acid pH TiO₂, 500 °C; (b) neutral pH TiO₂, 500 °C; (c) acid pH TiO₂, 650 °C; (d) neutral pH TiO₂, 650 °C.

3.2. Small electrodes

Fig. 5 displays the SEM micrographs of the four small, 1 cm^2 , thin-film electrodes formed by coating titanium plates with sol-gel TiO_2 . These pictures suggest that at equivalent temperatures of the heat treatment the acidic electrodes show smoother and more coherent surfaces, whereas neutral electrodes are rougher and more particulate.

The X-ray diffractograms of the three series of electrodes synthesized at acidic pH, neutral pH and iron-doped are shown in Fig. 6. Acid sol-gel electrodes show the presence of anatase crystals at 500°C which grow and progressively transform to rutile at 600°C and above. For calcination temperatures of 500, 600, 650 and 700°C , the average anatase crystal size are 10, 23, 30 and 68 nm, respectively.

In contrast, for neutral pH TiO_2 electrodes, and contrary to the results for the powders, no anatase crystalline phase was detected below 700°C although rutile lines were observed at 650°C . This implies that rutile crystals are not formed by transformation of an intermediate anatase to rutile phase but are directly formed. Iron doping did not modify this trend; at equivalent temperatures doped and undoped electrodes show very similar diffraction patterns. As these electrodes have been prepared by coating titanium plates, these results suggest that the rutile phase could be growing directly from the oxidation of the titanium support. Oxidation of the titanium metal would explain why the rutile signals are essentially equivalent in the three series, whereas anatase peaks strongly depends on the pH of the coating sol-gel solution. Moreover, in contrast with the results obtained for powder materials, the titanium substrate seems to inhibit anatase crystallization, favouring rutile formation. For neutral electrodes, the absence of defined anatase signals could be due to this destabilization of the anatase phase or to the fact that crystals are too small (below few nanometres) to produce detectable diffraction maxima, but form an optically and electrochemically active film, as will be shown afterwards.

Fig. 7a and b show the influence of the temperature, iron doping and pH on the photocurrent recorded in $0.1\text{ M Na}_2\text{SO}_4$ for these small thin-film TiO_2 electrodes. For the electrode fabricated by calcination at 500°C from TiO_2 synthesized at acid pH the current measured in $0.1\text{ M Na}_2\text{SO}_4$ was almost independent of voltage. This behaviour has been attributed previously to the fact that semiconductor particles are much smaller than the depletion layer width and consequently the electric field across the particle is too small to accelerate charge separation [13,23]. Increasing the electrode fabrication temperature to 650°C induces crystal growth to greater than 25 nm and the photocurrent is more dependent on voltage, as expected from the classical theory of semiconductor electrodes [38]. Although the neutral electrode showed a slight dependence of current on potential after 500°C calcination (perhaps because multiple calcinations had increased the crystallite size) it too showed a more pronounced voltage-dependence after calcination at 650°C . Since iron doping both increase the crystal size and reduces the depletion layer width, the photocurrent of the iron-doped electrodes is expected to be voltage dependent, and this indeed is the case. In all cases higher calcination temperatures increased the photocurrent recorded at positive potentials and the CV's of the acid electrodes are similar to those of the neutral ones, because of growth of the titania particles [26].

Fig. 7c and d show the cyclic voltammeteries of these electrodes in electrolyte plus 1 M methanol. Once again, all except the acid/ 500°C electrode show I - V curves in agreement with the classical semiconductor theory. The CV's of both the pure and the iron-doped neutral TiO_2 electrodes are quite similar to those in the

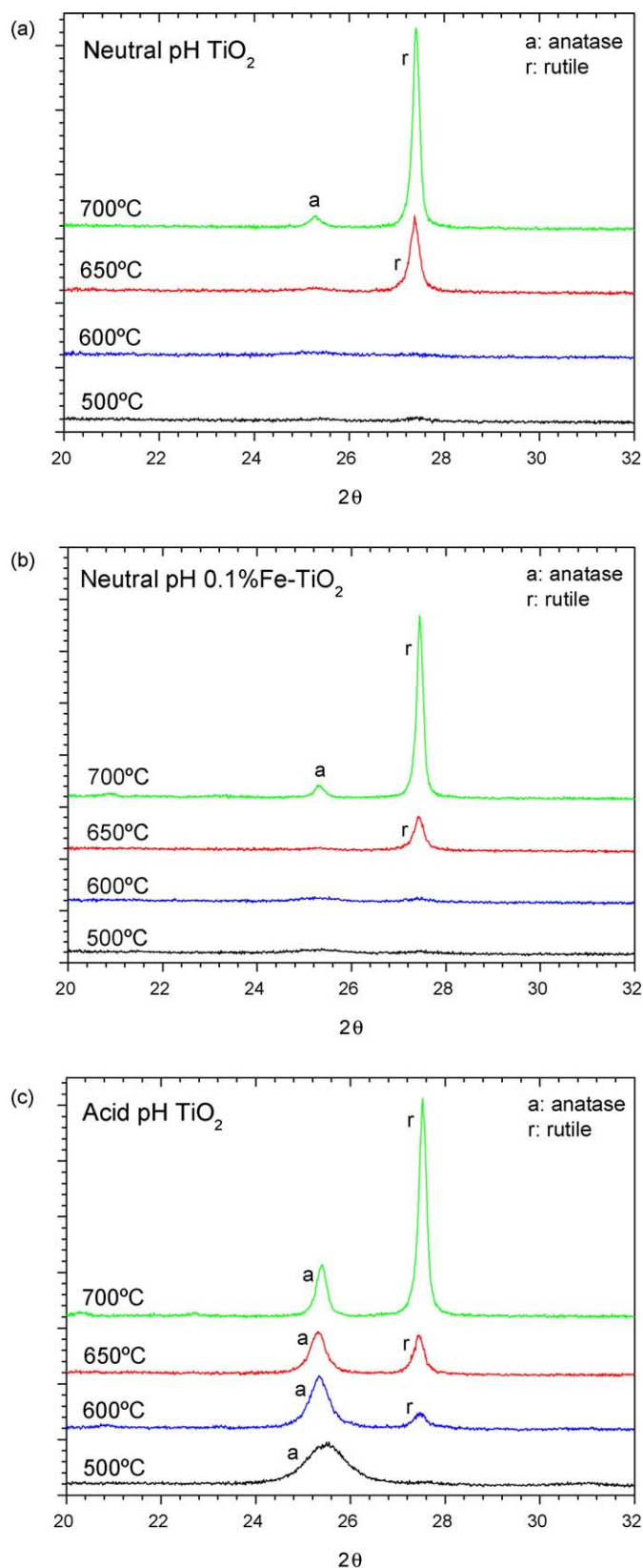


Fig. 6. Influence of temperature, iron doping and pH on the X-ray diffraction pattern of TiO_2 small electrodes, prepared under neutral (a and b) or acid (c) conditions.

absence of methanol. The photocurrents recorded for the acid TiO_2 electrodes are much higher, especially at lower calcination temperatures. To facilitate comparison Fig. 7e and f show the photocurrent increase resulting from methanol addition.

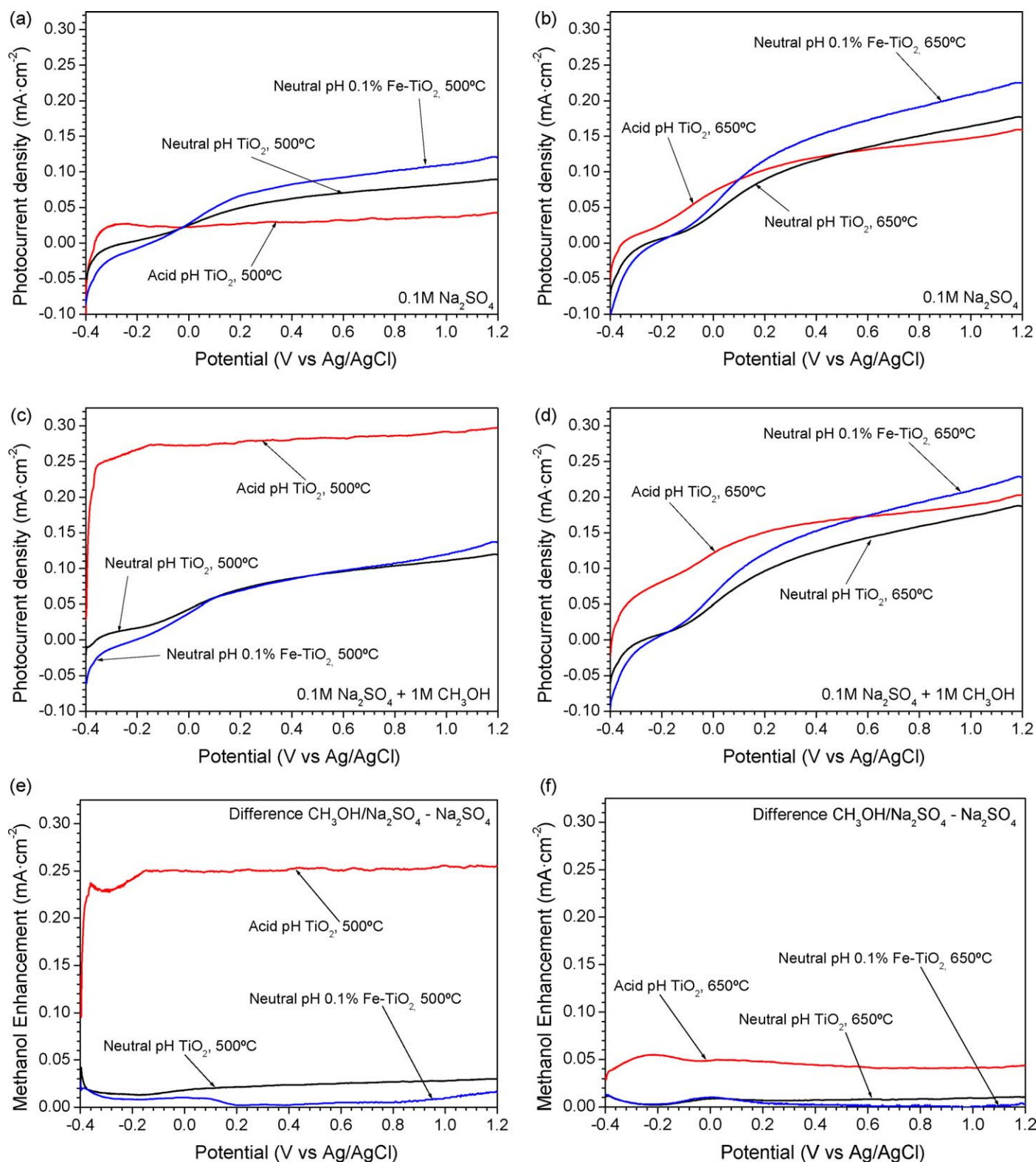


Fig. 7. Influence of temperature, iron doping and pH on the photocurrent density of TiO_2 electrodes in (a and b) 0.1 M Na_2SO_4 and (c and d) 0.1 M Na_2SO_4 + 1 M CH_3OH solutions. The enhancement due to methanol is shown in (e) and (f).

The influence of the electrode preparation temperature on the photocurrent at 1.0 V in Na_2SO_4 is shown in Fig. 8a; a photocurrent maximum is observed at 650 °C in all cases. The corresponding photocurrents in Na_2SO_4 /methanol (Fig. 8b) show an enhanced response of the acidic TiO_2 electrodes which decreases monotonically with increasing temperature until, it becomes compar-

able with those of neutral electrodes at 650 °C. As demonstrated in Fig. 8c, the photocurrent enhancement in methanol was negligible over the whole temperature range for the neutral electrodes, and decreased monotonically to zero, for the acid electrodes.

The photoelectrochemical properties of the undoped neutral electrodes are essentially unaffected by iron doping. Previous

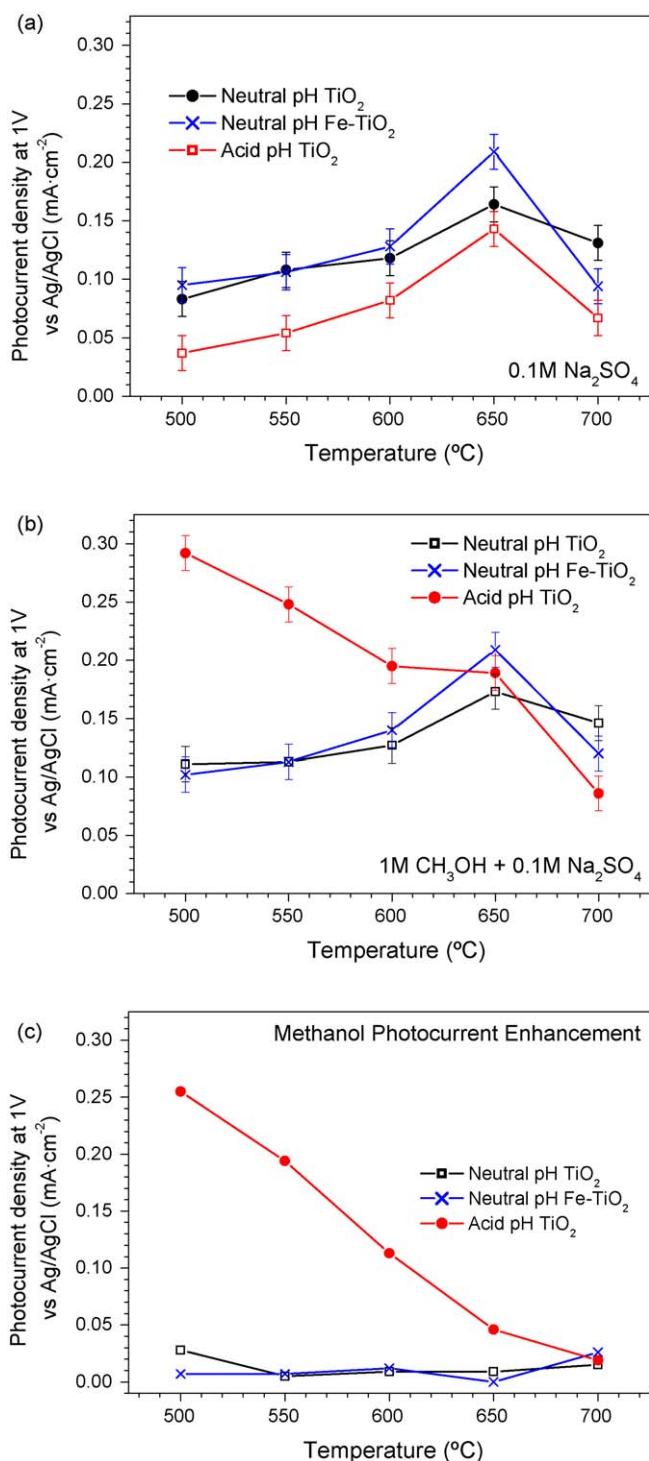


Fig. 8. Influence of temperature on the photocurrent density of TiO₂ electrodes: (a) 0.1 M Na₂SO₄; (b) 0.1 M Na₂SO₄ + 1 M CH₃OH; (c) methanol photocurrent enhancement.

results reported by Egerton et al. [22] showed that the photocurrent enhancement in the presence of methanol observed for sol-gel electrodes synthesized in acidic media disappears as the iron content in the doped titania increases. These results are in agreement with the vanishing of the photocurrent enhancement effect in photooxidation of 2-propanol on TiO₂ in solutions containing Fe(III) ions attributed by Ohno et al. [39] to a change to a two-hole oxidation mechanism on the Fe(III)-adsorbed TiO₂ surface.

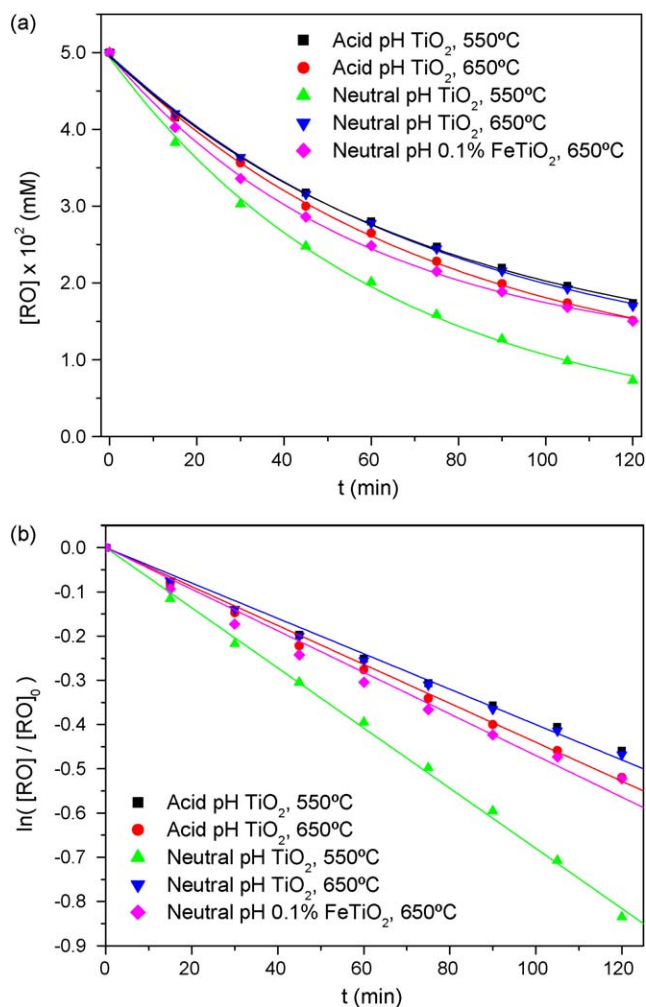


Fig. 9. Decolouration and derived first order kinetics fit of the R016 photoelectrocatalytic decolourisation with mesh electrodes at 1 V of potential bias.

Certain organic species in solution are well known to enhance the photocurrent of TiO₂ photoanodes [40]. This effect, known as current-doubling, is attributed to the injection of electrons into the conduction band by radical species formed upon oxidation of the organics by holes, and can double the apparent quantum efficiencies. However, the tenfold increase in the photocurrent recorded for acid electrodes calcined at 500 °C, and the null photocurrent enhancement for neutral electrodes, cannot be explained satisfactorily by a conventional current-doubling mechanism. The observed increase parallels the results of Fujishima and co-workers [41] on the effect of ethanol addition on the photocurrent of spray pyrolysed TiO₂ photoelectrodes. Fujishima et al. attributed the photocurrent enhancement in the presence of alcohol to suppression of the surface recombination processes at the TiO₂ photoelectrode. They considered the most probable explanation was that alcohol adsorbs at the TiO₂ surface and blocks the sites that would otherwise act as recombination. A similar proposal was made by Schoenmakers et al. [42] for the oxidation of methanol on single-crystal ZnO. In a study of photoelectrochemical oxidation of methanol in Na₂SO₄ solution John and co-workers [43] conclude that the limiting step was interfacial charge transfer and that the concentration of hydroxyl ions (the precursors of hydroxyl radicals) did not influence photocurrents at pH 9. This may be because methanol reacts more slowly than longer chain alcohols with hydroxyl radicals (typical second order rate constants of 4.7 and

Table 3

Synthesis conditions and activity of the large mesh electrodes at 1 V.

Name	Doping	pH	Temperature (°C)	k_{RO} (h ⁻¹)	External circuit current (mA)		
					0.1 M Na ₂ SO ₄	0.1 M Na ₂ SO ₄ + 1 M CH ₃ OH	Methanol enhancement
E-TiO ₂ -1	–	1.5	550	0.240	5.15	9.67	4.52
E-TiO ₂ -2	–	1.5	650	0.258	9.70	10.83	1.13
E-TiO ₂ -3	–	6.5	550	0.408	3.95	19.76	15.81
E-TiO ₂ -4	–	6.5	650	0.258	12.51	12.78	0.27
E-FeTiO ₂	0.1% Fe	6.5	650	0.228	17.72	18.86	1.14

$15 \times 10^8 \text{ M}^{-1} \text{ s}^{-1}$ [44]) – which is why methanol was selected for our experiments.

Suppression of the surface recombination processes in the presence of methanol would be especially important for very small titania crystals with high values of the surface-to-volume ratio. As the size of the crystals increases, the role of the volume recombination becomes more significant, and the effect of the suppression of the charge recombination in the surface would be negligible. The enhancement of the photocurrent of TiO₂ electrodes in the presence of organics has been previously reported [21,24,45] and attributed to the decrease in the charge recombination rate caused by the scavenging of the photogenerated holes. This effect is especially marked in rough particulate electrodes [24] and in microporous electrodes of high titania surface area [45], but negligible for thermal electrodes [21]. Consequently, it seems that electrodes prepared by coating with a neutral sol–gel suspension are more similar to thermal electrodes prepared by heating titanium plates than they are to particulate electrodes prepared for acidic sol–gel.

3.3. Large electrodes

Five large mesh electrodes were fabricated under conditions selected on the basis of the small-electrode results and summarized in Table 3.

Fig. 9 shows the photocatalytic activity for RO16 decolourisation by these mesh electrodes. In all cases the results were satisfactorily represented by pseudo-first order kinetics. The first order rate constants in Table 3 show that the neutral sol–gel electrode calcined at 550 °C had the highest photoelectrocatalytic activity for RO16 decolourisation.

Table 3 also shows the currents measured at 1 V (the value used for the photocatalytic reactions) both in 0.1 M Na₂SO₄ and 0.1 M

Na₂SO₄ + 1 M CH₃OH. In the absence of methanol the results are less influenced by the synthesis pH than by the thermal treatment temperature; at 550 °C, when the acid electrodes may be expected to have an anatase crystal size of ~15 nm the photocurrent is only slightly dependent on potential, at 650 °C for which X-ray line broadening suggested an anatase crystal size of 30 nm the photocurrent at 1 V has doubled for both acid and neutral undoped electrodes, i.e. the pattern is as for the smaller electrodes. The highest response for the undoped electrodes was for synthesis at pH 6.5 and calcination at 650 °C. Iron doping caused a clear increase of the recorded photocurrent, especially at higher potentials; again this is consistent with the decreased thickness of the double layer caused by higher dopant level.

Methanol addition significantly enhanced the photocurrent of undoped electrodes calcined at 550 °C, especially for the neutral electrode but did not significantly modify the photoelectrochemical behaviour of electrodes calcined at 650 °C. Again, this is consistent with the view that the enhancement due to methanol is mainly associated with small crystals. However, whereas for the small electrodes the greatest methanol enhancement was observed with the acid electrodes, in this case the enhancement is much bigger with the neutral electrodes. The TiO₂ crystallization procedure (and hence the electrode characteristics) has been shown, above, to be sensitive to the interaction with the titanium support. It is probably also sensitive to changes in heating and cooling rates brought about by changes in the thermal mass of the electrode. Moreover, the adhesion to the support can be strongly influenced by the type of electrode and synthesis conditions as suggested by the scanning electron microscopy observations. Fig. 10 appears to show that although a coherent film has formed on the wires from the acid sol–gel, it has fractured into 10–50 μm fragments many of which seem to be no longer adhering to the support. The neutral electrode shows a more

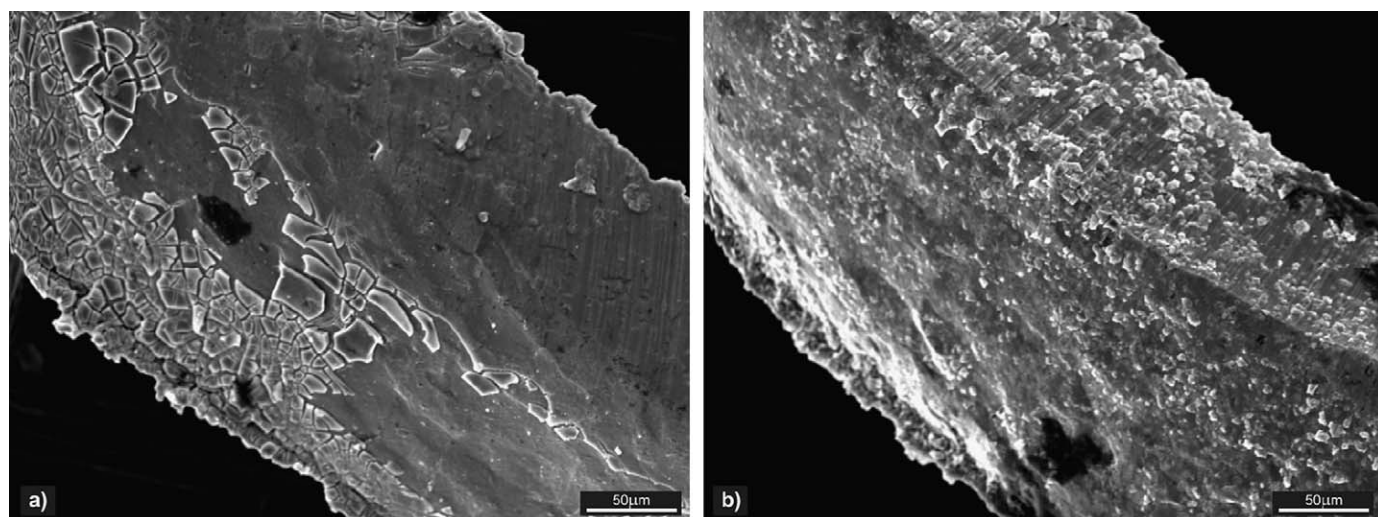


Fig. 10. SEM micrographs of mesh electrodes: (a) acid pH, 650 °C; (b) neutral pH, 650 °C.

highly granular coating, with most particles below 10 μm . However this granular coating appears to adhere much more strongly to the substrate. Such differences complicate the interpretation of photoelectrocatalytic properties measured on large-scale electrodes in terms of cyclic voltammetric measurements which for practical reasons must be made on small electrodes.

It is now well understood that photocatalysis by TiO_2 can occur either by formation of reactive hydroxyl radicals or be direct charge transfer [6]. Although it is possible that hydroxyl radicals may move from the oxide surface and therefore react with molecules in the gas phase, or in solution, direct charge transfer requires adsorption of the reactant onto the TiO_2 surface [46]. It is widely reported that the mechanism of degradation of complex dye [47], pesticide and herbicide molecules [48] involves adsorption and this view is supported by both, the widely reported increase in the rate of decolouration of anionic azo dyes such as reactive orange on positively charged TiO_2 surfaces and by the decrease in rate when at low pH values the negative charge on carboxylate molecules is suppressed [49]. The necessity for adsorption implies, but does not prove, that the degradation mechanism involves hole-transfer.

As discussed above, the increase in the photocurrent measured in the presence of methanol can be attributed to direct hole-transfer. For the large undoped electrodes, the highest methanol enhancement was found for the 550 °C neutral electrode and this electrode was the most active for dye decolouration. In the absence of methanol the iron doped electrode gave the highest photocurrent, whereas in the presence of methanol it gave a very modest photocurrent enhancement and also had the lowest activity for dye decolouration. These two observations support the view that dye decolouration proceeds by a direct hole-transfer mechanism.

4. Conclusions

The photoelectrocatalytic activity of TiO_2 electrodes is strongly conditioned by the synthesis procedure. The photocurrent of the electrodes and the activity for the decolouration of Reactive Orange 16 solutions is highly influenced by the pH of the coating titania sol and the temperature of the heat treatment.

In contrast, doping of TiO_2 with iron does not lead to major differences in the electrochemical or catalytic behaviour. Moreover, the role of iron seems to be the promotion of crystal growth (decrease of surface area) and the introduction of charge-carrier recombination centres leading to slightly worse photocatalytic activities. This contrast with previous results for bacteria disinfection [22], suggests that the effect of iron as recombination centres or as trapping sites that improve charge separation may depend on the specific mechanism of the photoelectrocatalytic reaction.

The significant increase in the photocurrent recorded in the presence of methanol for the electrodes synthesized at lower temperatures cannot be explained by a conventional current-doubling mechanism. Instead, this methanol photocurrent enhancement seems to be based on the suppression of the charge recombination, as postulated by Fujishima and co-workers [41]. This effect is especially important for very small titania crystals with a high surface-to-volume ratio, whereas for higher crystal sizes the volume recombination becomes more significant. The results of the RO16 photoelectrocatalytic decolouration show that a good correlation can be found between the activity of the electrodes and the photocurrent measured in the presence of methanol. This is consistent with dye decolouration proceeding by a direct hole-transfer mechanism.

Acknowledgements

JM gratefully acknowledges the financial support of the Ministerio de Educación y Ciencia of Spain through the program Consolider-Ingenio 2010 (project CSD2006-00044 TRAGUA) and Comunidad de Madrid through the program REMTAVARES S-0505/AMB/0395.

References

- [1] D.F. Ollis, H. Al-Ekabi (Eds.), *Photocatalytic Purification and Treatment of Water and Air*, Elsevier, Amsterdam, 1993.
- [2] D. Blake, Bibliography of work on the photocatalytic removal of hazardous compounds from water and air, NREL, Golden, CO; May 1994. Available at <http://www.nrel.gov> (1st update: October 1994; 2nd update: October 1996; 3rd update: January 1999; 4th update: October 2001).
- [3] M.R. Hoffmann, S.T. Martin, W. Choi, D.W. Bahnemann, *Chem. Rev.* 95 (1995) 69–96.
- [4] A. Mills, S. Le Hunte, *J. Photochem. Photobiol. A: Chem.* 108 (1997) 1–35.
- [5] J.M. Herrmann, *Catal. Today* 53 (1999) 115–129.
- [6] A.G. Agrios, P. Pichat, *J. Appl. Electrochem.* 35 (2005) 655–663.
- [7] D.S. Bhatkhande, V.G. Pangarkar, A.A. Beenackers, *J. Chem. Technol. Biotechnol.* 77 (2001) 102–116.
- [8] A. Mills, S.K. Lee, *Semiconductor photocatalysis*, in: S. Parsons (Ed.), *Advanced Oxidation Processes for Water and Wastewater Treatment*, IWA Publishing, London, UK, 2004.
- [9] J. Marugán, D. Hufschmidt, G. Sagawe, V. Selzer, D. Bahnemann, *Water Res.* 40 (2006) 833–839.
- [10] L. Sun, J.R. Bolton, *J. Phys. Chem.* 100 (1996) 4127–4134.
- [11] T.A. Egerton, P.A. Christensen, *Photoelectrocatalysis processes*, in: S. Parsons (Ed.), *Advanced Oxidation Processes for Water and Wastewater Treatment*, IWA Publishing, London, UK, 2004.
- [12] T.A. Egerton, P.A. Christensen, S.A.M. Kosa, B. Onoka, J.C. Harper, J.R. Tinlin, *Int. J. Environ. Pollut.* 27 (2006) 2–19.
- [13] K. Vinodgopal, U. Stafford, K.A. Gray, P.V. Kamat, *J. Phys. Chem.* 98 (1994) 6797–6803.
- [14] P. Fernandez-Ibañez, S. Malato, O. Enea, *Catal. Today* 54 (1999) 329–339.
- [15] J.A. Byrne, A. Davidson, P.S.M. Dunlop, B.R. Egging, *J. Photochem. Photobiol. A: Chem.* 148 (2002) 365–374.
- [16] P.A. Carneiro, M.E. Osugi, J.J. Sene, M.A. Anderson, M.V. Boldrin Zanoni, *Electrochim. Acta* 49 (2004) 3807–3820.
- [17] P.A. Christensen, T.A. Egerton, S.A.M. Kosa, J.R. Tinlin, K. Scott, *J. Appl. Electrochem.* 35 (2005) 683–692.
- [18] G. Waldner, J. Krýsa, *Electrochim. Acta* 50 (2005) 4498–4504.
- [19] T.A. Egerton, H. Purnama, S. Purwajanti, M. Zafar, *J. Adv. Oxid. Technol.* 9 (2006) 79–85.
- [20] J. Georgieva, S. Armanov, E. Valova, I. Poullos, S. Sotiropoulos, *Electrochem. Commun.* 9 (2007) 365–370.
- [21] P.A. Christensen, T.P. Curtis, T.A. Egerton, S.A.M. Kosa, J.R. Tinlin, *Appl. Catal. B: Environ.* 41 (2003) 371–386.
- [22] T.A. Egerton, S.A.M. Kosa, P.A. Christensen, *Phys. Chem. Chem. Phys.* 8 (2006) 398–406.
- [23] J.C. Harper, P.A. Christensen, T.A. Egerton, T.P. Curtis, J. Gunlazuardi, *J. Appl. Electrochem.* 31 (2001) 623–628.
- [24] I. Mintsouli, N. Philippidis, I. Poullos, S. Sotiropoulos, *J. Appl. Electrochem.* 36 (2006) 463–474.
- [25] J. Aguado, R. van Grieken, M.J. López-Muñoz, J. Marugán, *Appl. Catal. A: Gen.* 312 (2006) 202–212.
- [26] J. Marugán, P. Christensen, T. Egerton, H. Purnama, *Int. J. Photoenergy* 1 (2008), doi:10.1155/2008/759561.
- [27] W. Choi, A. Termin, M.R. Hoffmann, *J. Phys. Chem.* 98 (1994) 13669–13679.
- [28] B. O'Regan, J. Moser, M. Anderson, M. Graetzel, *J. Phys. Chem.* 94 (1990) 8720–8726.
- [29] H. Zhang, J.F. Banfield, *J. Phys. Chem. B* 104 (2000) 3481–3487.
- [30] C.-C. Wang, J.Y. Ying, *Chem. Mater.* 11 (1999) 3113–3120.
- [31] A.A. Gibb, J.F. Banfield, *Am. Mineral.* 82 (1997) 717–728.
- [32] J.A. Navío, G. Colón, M. Macías, C. Real, M.I. Litter, *Appl. Catal. A: Gen.* 177 (1999) 111–120.
- [33] J.C. Colmenares, M.A. Aramendía, A. Marinas, J.M. Marinas, F.J. Urbano, *Appl. Catal. A: Gen.* 306 (2006) 120–127.
- [34] I.-K. Kim, H.-J. Ha, S.-K. Lee, J.-K. Lee, *Kor. J. Chem. Eng.* 22 (2005) 382–386.
- [35] X.H. Wang, J.-G. Li, H. Kamiyama, Y. Moriyoshi, T. Ishigaki, *J. Phys. Chem. B* 110 (2006) 6804–6809.
- [36] J. Feng, R.S.K. Wong, X. Hu, P.L. Yue, *Catal. Today* 98 (2004) 441–446.
- [37] C. Adan, A. Bahamonde, M. Fernández-García, A. Martínez-Arias, *Appl. Catal. B: Environ.* 72 (2007) 11–17.
- [38] A. Hamnett, *Compr. Chem. Kinet.* 27 (1987) 61–246.
- [39] T. Ohno, S. Izumi, K. Fujihara, Y. Masaki, M. Matsumura, *J. Phys. Chem. B* 104 (2000) 6801–6803.
- [40] T. Freund, W.P. Gomes, *Catal. Rev.* 3 (1969) 1–36.
- [41] O.A. Semenikhin, V.E. Kazarinov, L. Jiang, K. Hashimoto, A. Fujishima, *Langmuir* 15 (1999) 3731–3737.

- [42] G.H. Schoenmakers, D. Vanmaekelbergh, J.J. Kelly, J. Chem. Soc. Faraday Trans. 93 (1997) 1127–1132.
- [43] D. Jiang, H. Zhao, Z. Jia, J. Cao, R. John, J. Photochem. Photobiol. A: Chem. 144 (2001) 197–204.
- [44] B. Halliwell, J.M.C. Gutteridge, *Free Radicals in Biology and Medicine*, 2nd ed., Oxford University Press, Oxford, UK, 1989.
- [45] J.A. Byrne, B.R. Eggins, J. Electroanal. Chem. 457 (1998) 61–72.
- [46] A.G. Agrios, P. Pichat, J. Photochem. Photobiol. A: Chem. 180 (2006) 130–135.
- [47] C. Guillard, H. Lachheb, A. Houas, M. Ksibi, E. Elaloui, J.M. Herrmann, J. Photochem. Photobiol. A: Chem. 158 (2003) 27–36.
- [48] M. El Madani, C. Guillard, N. Perol, J.M. Chovelon, M. El Azzouzi, A. Zrineh, J.M. Herrmann, Appl. Catal. B: Environ. 65 (2006) 70–76.
- [49] M. Carrier, N. Perol, J.M. Herrmann, C. Bordes, S. Horikoshi, J.O. Paise, R. Baudot, C. Guillard, Appl. Catal. B: Environ. 65 (2006) 11–20.